Available online at www.sciencedirect.com
ScienceDirect
International Journal of Heat and Mass Transfer 51 (2008) 2940–2949
International Journal of HEAT and MASS TRANSFER
www.elsevier.com/locate/ijhmt

Effects of a reacting channel wall on turbulent mass transfer

Kien T. Nguyen [a], Dimitrios V. Papavassiliou [a,b,*]

[a] School of Chemical, Biological and Materials Engineering, The University of Oklahoma, 100 East Boyd, Norman, OK 73019, USA
[b] Sarkeys Energy Center, The University of Oklahoma, 100 East Boyd, Norman, OK 73019, USA

Received 11 June 2007; received in revised form 10 September 2007
Available online 13 November 2007

Abstract

The effects of a turbulent fluid reacting with the channel wall on the turbulent mass transfer were investigated using a Lagrangian method. The reactants diffused from the bulk of the fluid to the channel walls, where they reacted by an effectively first-order reaction. The effective reaction rate was found to be diffusion limited for high Schmidt number fluids. The mass transfer coefficient was found to be independent of reaction rate, but was found to exhibit a strong dependence on the Schmidt number. A correlation of the mass transfer coefficient as a function of the Schmidt number for both low and high Schmidt numbers was obtained.

Keywords: Turbulence; Dispersion; Mass transfer; Reactive flow; Lagrangian simulation methods

1. Introduction

Turbulent scalar transport plays a crucial role in many industrial applications, including the design of reactors, heat exchangers, and mixing tanks. The interactions of chemical reactions, fluid mechanics, and mass transfer have been recognized for decades, but the investigation of interacting turbulent transport phenomena theoretically, experimentally and numerically is limited, at least in numbers, relative to the literature on turbulent flow. In engineering practice, the usual numerical approach to turbulent transport is to apply a form of the Reynolds analogy to relate eddy viscosity to eddy diffusivity, and to apply a second-order closure for the turbulent momentum and heat balance equations written in their Reynolds averaged form [1–3]. Sophisticated numerical techniques, like large eddy simulation (LES) and direct numerical simulation (DNS), have also been used to investigate turbulent heat transfer [4,5] in the Eulerian framework. In the study presented here, the flow effects on the turbulent mass transfer between a turbulent fluid and a smooth, flat channel wall, with the presence of a first-order reaction, are investigated using a Lagrangian method (Lagrangian scalar tracking, LST). The turbulent flows are generated using DNS.

Previous efforts to investigate the effects of a chemical reaction on turbulent mass transfer include the work of Kader and Gukhman [6], who developed an analytical solution for the mass transfer from a turbulent fluid flow to a long, smooth, and flat wall with a first-order reaction using a boundary-layer approximation. Hanna et al. [7] employed a large Schmidt number asymptotic approximation procedure to derive an analytical solution for the mass transfer from the wall accompanied by a first-order chemical reaction for liquids in fully developed turbulent flow in a circular tube. Meyerink and Friedlander [8] and Harriott and Halmilton [9] have conducted experiments to measure the mass transfer rate of benzoic acid, which dissolved from the wall of a pipe into water or glycerine–water solution in fully developed turbulent flow. Riley et al. [10] performed direct numerical simulations of chemically reacting, turbulent mixing layers with a binary, irreversible reaction with no heat release. Leonard and Hill [11] carried out full turbulent simulations using a pseudo-spectral method in 32^3 and 64^3 domains with the presence of a second-order reaction. Mitrovic and Papavassiliou [12] studied the effects

* Corresponding author. Address: School of Chemical, Biological and Materials Engineering, The University of Oklahoma, 100 East Boyd, Norman, OK 73019, USA. Tel.: +1 405 3255811; fax: +1 405 3255813.
E-mail address: dvpapava@ou.edu (D.V. Papavassiliou).

0017-9310/$ - see front matter © 2007 Elsevier Ltd. All rights reserved.
doi:10.1016/j.ijheatmasstransfer.2007.09.028

Nomenclature

b	first coefficient of the Taylor expansion of K_{yy}
c	concentration
c'	concentration fluctuation
C_0	average concentration at the entrance
D	molecular diffusivity
h	half-height of the channel
H	distance of a heat marker from the channel wall
J	mass flux
K	mass transfer coefficient
k	reaction rate coefficient
K_{ij}	tensor component of eddy diffusivity
l^*	characteristic length scale, $l^* = \nu/u^*$
n	bin number or parameter in Eq. (12)
p	probability that a mass marker colliding with the wall reacts with the wall
P	standard normal probability distribution function
P_1	conditional probability for a marker to be at a location (x, y) at time t, given that it was released at a known time from a known location in the channel
p_P	Poisson probability, the probability that any mass marker in the flow field react with the wall
Re	Reynolds number, $Re = Uh/\nu$
Sc	Schmidt number, $Sc = \nu/D$
Sh	Sherwood number, $Sh = 4ScK^+h^+$
t^*	characteristic time scale, $t^* = \nu/(u^*)^2$, $t^* = 1$ for DNS
t	time
t_0, t_f	initial and final time of tracking markers
$t_{1/2}$	half-life of the first-order reaction
U	centerline mean velocity
u^*	friction velocity, $u^* = (\tau_w/\rho)^{1/2}$
u, v, w	velocity in the x, y, and z directions
x, y, z	streamwise, normal, and spanwise coordinates
X, Y	Lagrangian displacement of a marker from the source in the x, y directions
Z	standard normal distribution function variable

Greek symbols

ν	kinematic viscosity
ρ	fluid density
σ	standard deviation of a probability density function
τ	shear stress
Δt	time step
Δx, Δy	bin size in x, y direction

Subscripts and superscripts

$\overline{()}$	time-averaged value
$\vec{()}$	vector quantity
$()^+$	value made dimensionless with viscous wall parameters
$()'$	fluctuating quantity
$()^\circ$	value at stabilized conditions
$()_b$	bulk value
$()_{\text{eff}}$	effective value
$()_w$	value at the wall of the channel
$()_0$	value at the entrance of the channel
$()_\infty$	value at infinity

of a first-order chemical reaction on turbulent mass transfer from a wall to the bulk using Lagrangian methods (LST). In that study, mass markers were released from the wall to a turbulent flow field generated using DNS and transformed to a product later in time using a Poisson probability function to describe the rate of reaction. The mass markers used in Ref. [12] were passive and did not affect the flow. For the case of heavy particles simulated with Lagrangian methods see [13], and references therein.

The interactions of chemical reactions and transport in tubular reactors have usually been ignored in textbooks and engineering software with the assumption of a plug flow reactor, in which the effects of velocity and temperature distribution in the direction normal to the vessel walls on the rate of reactions are not taken into account. A bright exception to this trend is the work of Churchill and coworkers, who investigated the interactions of chemical reactions and transport using generalization and asymptotic methods, and developed design equations for tubular reactors, in which the effects of radial variations on the rate of reaction were taken into consideration [14,15].

The problem presented here and the problem reported by Kader and Gukhman [6] are similar. In both of them, the reactants diffuse from a turbulent fluid flow to a long, flat, and smooth wall, and react with the wall by a first-order reaction. The LST methodology is used with the goal of exploring the effects of the turbulence on the mass transfer and on the effective reaction rate. This problem can be important for applications like electrodiffusional sensors and semiconductor manufacturing.

2. Background - turbulent mass transfer in the Eulerian framework

In the Eulerian description of turbulent transport, a scalar is decomposed into a time-averaged value and a fluctuation. For mass concentration, it is $c = \bar{c} + c'$. The steady state diffusion equation with no reaction, for 2D flows, is of the following form:

$$\bar{u}(y)\frac{\partial \bar{c}}{\partial x} = D\left(\frac{\partial^2 \bar{c}}{\partial x^2} + \frac{\partial^2 \bar{c}}{\partial y^2}\right) - \frac{\partial}{\partial x}\left(\overline{u'c'}\right) - \frac{\partial}{\partial y}\left(\overline{v'c'}\right) \tag{1}$$

When the fluid reacts on the surface of the channel wall, the effective reaction rate can be represented with a first-order reaction at the wall. The mass flux near the wall has to be equal to the rate of reaction at the wall

$$D\left(\frac{\partial \bar{c}}{\partial y}\right)_w = k\bar{c}_w \tag{2}$$

Making Eq. (2) dimensionless using viscous wall parameters and evaluating it at the wall yields

$$\frac{1}{Sc}\left(\frac{\partial \bar{c}}{\partial y^+}\right)_w = k\overline{c_w} \tag{3}$$

The mass flux at the wall in the y-direction is given by

$$J_w = K(\overline{c_b} - \overline{c_w}) \tag{4}$$

The dimensionless mass transfer coefficient, which is defined as $K^+ = K/u^*$, where u^* is the friction velocity, can be calculated using the following equation:

$$K^+ = \frac{1}{Sc}\left[\frac{\mathrm{d}(\bar{c}/(\overline{c_b} - \overline{c_w}))}{\mathrm{d}y^+}\right]_w \tag{5}$$

Using the LST method, Mitrovic et al. [16] obtained the following limiting expressions for the mass transfer coefficient for fully developed flow in a channel with a constant mass flux from the wall and without any reaction:

$$K^+ = 0.0465 \cdot Sc^{-0.510} \quad \text{for} \quad Sc \leqslant 10 \tag{6a}$$

$$K^+ = 0.0835 \cdot Sc^{-0.690} \quad \text{for} \quad Sc \geqslant 100 \tag{6b}$$

By approximating the tensor components of the eddy diffusivity by the first term of the corresponding Taylor power expansion, Kader and Gukhman [6] have developed an expression for the mass transfer from a turbulent fluid flow to a long, smooth, and flat wall with the presence of a first-order reaction and obtained expressions of K^+ for the case of $Sc \gg 1$ and infinitely fast reaction rate (i.e. $k \to \infty$), as follows:

$$K^+ = \frac{3\sqrt{3}}{2\pi}\sqrt[3]{b}Sc^{-2/3} \tag{7}$$

The ratio of the Sherwood number at any position along the length of the channel, Sh, divided by the Sherwood number at the stabilized condition, Sh^0, was also estimated as

$$\frac{Sh}{Sh^0} = \frac{1}{\sqrt[1/3]{1 - \exp(-3.62bx^+)}} \tag{8}$$

Even though the above two equations provide a representation of the conductive sublayer where molecular diffusivity is dominant, since only the first term of the Taylor expansion was used, the equations can be used to provide a good approximation to the expected behavior of the mass transfer coefficient and the Sh.

3. Simulation of a first-order chemical reaction with a Lagrangian scalar tracking method

Direct numerical simulation methods for the simulation of turbulent flow fields do not model any terms of the Navier–Stokes equation. Therefore, DNS is a precise and reliable method of simulating turbulent flows. Lagrangian scalar tracking is a methodology that utilizes a tracking algorithm that monitors the space-time trajectories of heat/mass markers in a flow field generated by a DNS. Because of the difficulties in conducting experiments measuring the trajectories of reactants in a turbulent flow field, a computational approach, like LST, is easier to perform and can be feasible with the advancement of supercomputing. In the turbulent flow field, a mass marker's motion can be decomposed into a convective part and a molecular diffusion part. The convective part can be calculated from the fluid velocity at the marker position, which is obtained from the DNS velocity field using a high order interpolation scheme [17]. The molecular motion after each time step, Δt, is calculated with a random jump from a Gaussian distribution with zero mean and standard deviation, $\sigma = \sqrt{2\Delta t^+/Sc}$, for each one of the three space dimensions in viscous wall units (this follows from Einstein's theory for Brownian motion [18]). Details about the implementation and validation of the LST methodology, including the stochastic tracking of markers in a turbulent flow field and the statistical post-processing of the results to obtain scalar profiles, can be found in Refs. [16,19–28]. A rather brief description is offered below, with most emphasis on the simulation methodology for surface reactions.

The building block for the Lagrangian formulation is the conditional probability density function $P_1(X - x_0, Y, t - t_0|\vec{x_0}, t_0)$ for a marker which is released at x_0 at time t_0 to be at a location (X, Y) at time t. This probability can be interpreted physically as concentration [22,24,29], or a snapshot of a cloud of contaminants released instantaneously from $x_0 = 0$ at $t_0 = 0$. Integrating (or, in the discrete case, summing up) P_1 from time t_0 to a final time t_f generates the behavior of a continuous source at the entrance of the channel, a source with a constant mass flux, which represents the mean concentration in the channel

$$\overline{C}(X - x_0, Y) = \sum_{t=t_0}^{t_f} P_1(X - x_0, Y, t|\vec{x_0}, t_0) \quad \text{with} \quad t_f \to \infty \tag{9}$$

A schematic of the problem is shown in Fig. 1. The flow is between two infinite planes and the flow simulation is conducted on a $128 \times 65 \times 128$ grid in x, y, and z directions for the DNS. The x axis is along the direction of the flow while y is the direction normal to the wall. The half-channel height, h^+, is 150 in dimensionless viscous wall units. The dimensions of the computational box are $4\pi h \times 2h \times 2\pi h$. The flow is periodic in the x and z directions, with periodicity lengths equal to the dimensions of the computational box in these directions. The DNS used has been validated quite thoroughly in previous work [30,31]. After the fluid flow reached fully developed, stationary state, the reactant mass markers were released into the fluid flow. This is analogous to the case of a well-mixed reactant solution in the flow approaching a section of the

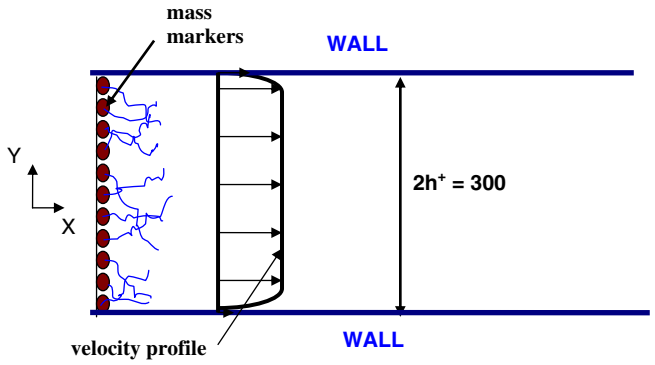

Fig. 1. This figure shows the *xy* cross-section of the channel with a first-order reaction and how mass markers are released into the flow field.

wall where the solution can deposit, similar to a chemical vapor deposition (CVD) case, or where the wall reacts with the solution. The mass markers can diffuse from the bulk fluid to the wall and react with the wall. The reaction equation can be written as: A → B, where A is the reactant and B is the product, which is adsorbed by the wall. The Reynolds number, *Re*, based on the mean centerline velocity and the half-channel height of the turbulent flow field is 2660. In order to simulate these conditions, 145,161 mass markers were released into the turbulent flow field instantaneously along the cross-section at the entrance of the channel as shown in Fig. 1. The release locations were distributed randomly in the *yz* cross-section of the channel.

When a marker would collide with the wall, a reflective boundary condition was applied. The trajectories of all mass markers were calculated as a function of time, and stored for post-processing. Since the same data for marker trajectories were used to simulate different reaction rates, the information about marker collisions with the wall were not saved during production runs. Instead, the effects of the reaction were calculated as part of the post-processing of the data for the marker trajectories, as described below.

The first step was to determine whether a marker collided with the wall or not within a time step. Consider that when a mass marker is close enough to the wall, it can move towards the wall and collide with the wall or it can move away from the wall. Assuming that very close to the wall ($y \to 0$) any meaningful marker movement in the *y*-direction is due to molecular diffusion, the random movement in the *y*-direction follows a normal distribution, which has a mean of zero and a standard deviation, $\sigma = \sqrt{2\Delta t^+/Sc}$. Therefore, the probability that a mass marker, which is close enough to the wall (at a distance H from the wall), collides with the wall can be calculated knowing H and σ. If Δy is the random jump of that marker in the *y*-direction in the next time step, the probability that the marker will collide with the wall in the next time step is the probability that Δy is equal to or larger than H, or $1 - P(H \leqslant \Delta y/\sigma)$, where the cumulative probability P for a standard normal distribution function is given by

$$P\left(Z \leqslant \frac{\Delta y}{\sigma}\right) = \int_{-\infty}^{\frac{\Delta y}{\sigma}} \frac{1}{\sqrt{2\pi}} e^{-x^2/2} dx \tag{10}$$

A random check was therefore conducted along the trajectory of every marker to determine whether the marker collided with the wall or not.

One way to validate this approach is to make sure that it yields zero mass concentration at the wall when the reaction is instantaneous. The wall concentration was calculated by extrapolating the concentrations at several positions close to the wall in the viscous sub layer where it is assumed that the concentration profile is linear [16,28]. It turned out that for high Schmidt number flows ($Sc \geqslant 50$), zero wall concentration was obtained. However, for smaller Schmidt number flows ($Sc \leqslant 10$), the wall concentrations calculated were positive. Thus, the post-processing method described above underestimates the number of collisions, because it neglects the effect of convective motions of the mass markers at the time step before collision with the wall, an effect that can be important for small *Sc*. Therefore, the probability of collision calculated by this method was multiplied with a correction factor, which was calculated to be 1.12. This correction factor is the smallest correction factor that guaranteed to yield zero wall concentration for the smallest Schmidt number flow investigated ($Sc = 0.1$).

The second step of the algorithm was to determine the collisions that result in reaction. When a mass marker collides with the wall, it has a chance to react with the wall and get adsorbed by the wall. The probability that a marker on the wall reacts with the wall is called the reaction probability, p. This probability determines the nominal reaction rate, and can be related to the first-order reaction half-time as $t_{1/2} = \ln(0.5)/\ln(1-p)$. In this study, *Sc* was varied from 0.1 (gas) to 1000 (ionic liquid solution), and p was varied from 0 (no reaction) to 1 (instantaneous reaction). Specifically, $Sc = 0.1$, 0.7, 6, 10, 50, 100, 500, and 1000; $p = 0.1$, 0.25, 0.5, 0.75, and 1.0. The time step in the simulation was set to $\Delta t^+ = 0.25$ in viscous wall units, and each simulation was carried out to a final time of 1500 viscous wall units. Four simulations were conducted for each *Sc* and p case, each one with different initial velocity field, as discussed in Section 4.1 below.

4. Results and discussion

4.1. Concentration profiles

Fig. 2 shows the normalized mass concentration contour on a 2-D cross-section of the channel up to $x^+ = 6000$ with $p = 0.1$ and $p = 1.0$ for the case of $Sc = 0.1$ (low *Sc*) and $Sc = 100$ (high *Sc*). In order to calculate the mass concentration, the channel was divided into bins with a height $\Delta y^+ = 1.0$ and an initial length $\Delta x^+ = 15.0$. Higher resolution was used near the channel entrance. The bin length at the entrance was 15.0, but it increased by a factor of 1.08 for subsequent bins in the *x*-direction. Therefore, the bins

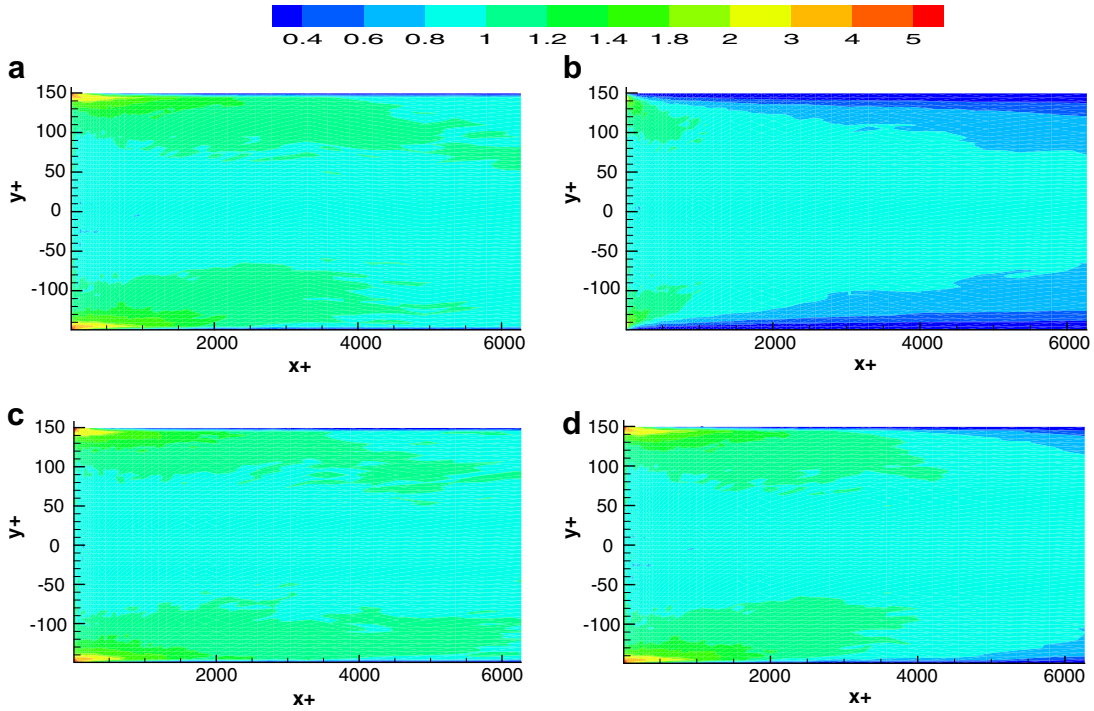

Fig. 2. Concentration contours for four cases: (a) $Sc = 0.7$, $p = 0.1$ (b) $Sc = 0.7$, $p = 1.0$ (c) $Sc = 100$, $p = 0.1$ (d) $Sc = 100$, $p = 1.0$. The concentration is normalized with the concentration at the channel entry, at $x_0 = 0$.

in column n had a length of $15.0 \times 1.08^{n-1}$. The mass concentration was defined based on the number of mass markers per unit area. Fig. 2 shows the mass concentration normalized by the concentration at the entrance of the channel, C_0.

Since the mean fluid velocity is higher in the middle section of the channel than the velocity near the wall, the mass markers in the middle of the channel can move faster in the streamwise direction than those near the wall. Because of this velocity profile, and the fact that the mass markers are uniformly distributed over the channel cross-section at the plane of their release ($x = x_0$), there is significant accumulation of mass markers near the walls close to the channel entrance. This creates very high concentration near the walls and lower concentration in the middle of the channel, resulting in mass transfer from the wall region towards the center of the channel. This is an entrance-effect, and the region affected by this is the *entrance-effect region*. Beyond the entrance-effect region, the effects of the surface reaction become prominent, and the concentration near the walls is much lower than that in the middle of the channel, as shown in the contour plots. The length of the entrance-effect region increases with higher Sc and lower p. As shown in Fig. 2, for the $Sc = 0.7$, $p = 1.0$ case, the entrance-effect extends to $x^+ = 800$, while for the $Sc = 100$, $p = 0.1$ case, the effect extends to $x^+ = 5200$. It can also be seen that the overall concentration and the concentration near the wall is lower for lower Sc and higher p. This is expected, because for lower Sc, the mass markers can diffuse faster to the wall due to larger molecular diffusion movements, which leads to a faster reaction closer to the marker release plane. Higher reaction probability also makes the reaction faster. Finally, a faster reaction will take more mass markers out of the flow field and lower both the overall concentration and the concentration near the wall at specific distance from the marker entry point.

The contour plots in Fig. 2 show data noise. The concentration contours are not symmetric across the center line of the channel, as expected. In order to reduce the noise, four different simulations were performed for each set of Sc and p, each with different initial fluid flow velocities. The average of the results of these four simulations was calculated, and all the results presented from this point and on (the mass transfer coefficient, the effective reaction rate constant, etc.) are these averaged results. Furthermore, for each simulation, the results were the average of the calculations for the top channel wall and the bottom channel wall.

4.2. Mass transfer coefficient

The mass transfer coefficient as a function of the distance from the channel entry can be calculated using Eq. (5). The dimensionless mass transfer coefficient K^+ as a function of Sc and channel length is shown in Fig. 3 with $p = 1.0$ (instantaneous reaction) and a wide range of Sc. There is a strong dependence of K^+ on Sc. Larger K^+ was observed for lower Sc. This is expected, because in lower Sc flows, the mass markers have larger molecular diffusion and, therefore, can diffuse faster to the wall. The entrance-effect was observed for all Sc numbers with K^+ much larger near the entrance, but then K^+ drops quickly

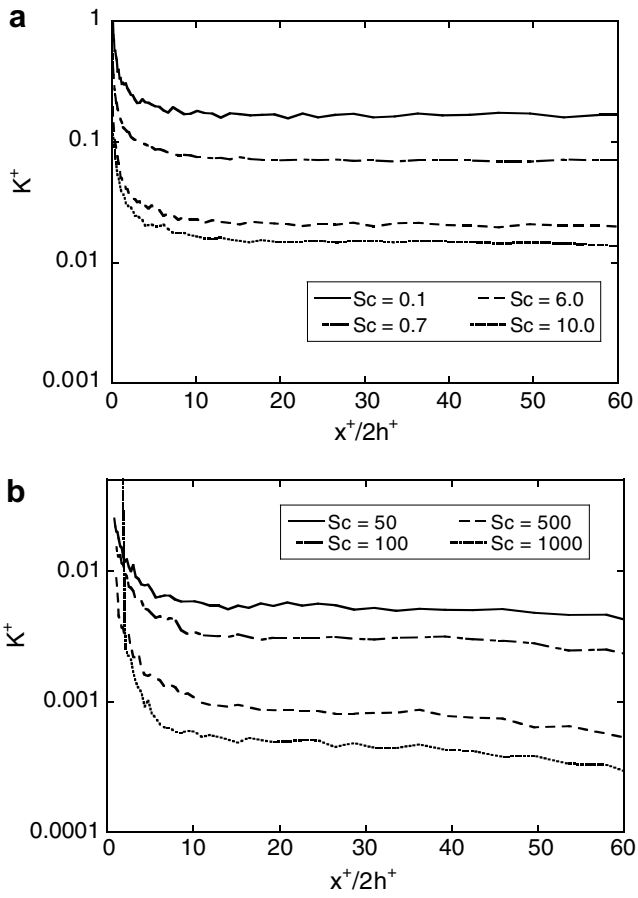

Fig. 3. The dimensionless mass transfer coefficient for the case of instantaneous reaction as a function of channel length for (a) lower *Sc*, and (b) higher *Sc*.

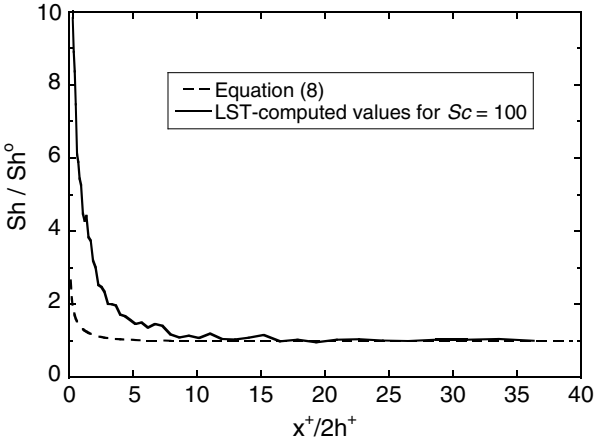

Fig. 4. The LST-computed and Kader and Gukhman's [6] results for Sh/Sh_0 for the case of instantaneous reaction.

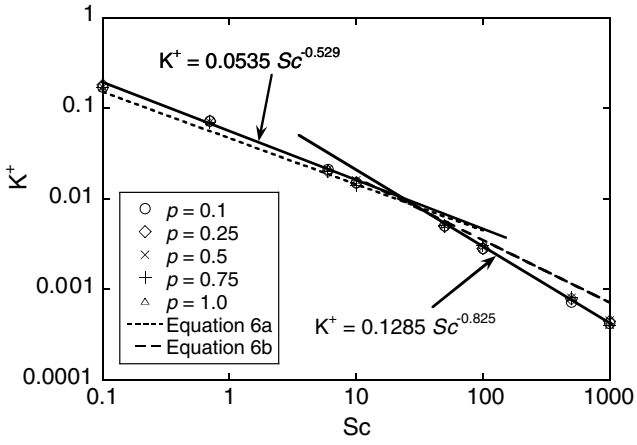

Fig. 5. Dimensionless mass transfer coefficient as a function of *Sc* and reaction probability.

and stabilizes (i.e., reaches a plateau) at around $x^+/2h^+ = 10$. Note that the values of the mass transfer coefficient, as defined in Eq. (5), are negative at very small distances from the entrance, because the concentration in the bulk is smaller than the wall concentration (see for example Fig. 2a and $x^+ \leqslant 500$). These negative values were not plotted on Fig. 3. The computed values of the stabilized K^+ are in good agreement with Kader and Gukhman's analytical results [6] for the asymptotic case of infinitely fast reaction and high *Sc*. For $Sc = 10.0$, Eq. (7) gives $K^+ = 0.0141$ and the LST-computed K^+ value is 0.015. For $Sc = 100$, Eq. (7) gives $K^+ = 0.00305$, while the computed K^+ value is 0.003. The ratio of the Sherwood number at any position along the length of the channel, *Sh*, divided by the Sherwood number at the stabilized condition, Sh^0, and how that compares to the results of Kader and Gukhman [6] (Eq. (8)) is shown in Fig. 4. The numerical results show that the entrance-effects are much stronger than in the analytical results. Both numerical and analytical results show that the mass transfer coefficient reaches a plateau downstream.

In order to study the effects of *Sc* and *p* on turbulent mass transfer, K^+ is plotted as a function of these two variables, as shown in Fig. 5. The mass transfer coefficient for the case of a fully developed flow in a channel with a constant mass flux from the wall without any reaction, which is given by Eq. (6), as a function of *Sc* is also plotted in Fig. 5. The effect of *Sc* on K^+ is significant. It can be observed that K^+ follows two different dependencies on *Sc*, one for $Sc \leqslant 10$ and one for $Sc \geqslant 50$. Table 1 shows the correlations of K^+ as a function of *Sc* for different values of *p*. The correlations of K^+ as a function of *Sc* with averaged parameters are:

$$K^+(Sc) = 0.0535 Sc^{-0.529} \quad \text{for} \quad Sc \leqslant 10 \tag{11a}$$

$$K^+(Sc) = 0.1285 Sc^{-0.825} \quad \text{for} \quad Sc \geqslant 50 \tag{11b}$$

The effect of reaction probability on K^+ is very small and does not follow any trend. Therefore, it is concluded that K^+ is independent of the reaction rate. The value of the exponent for low *Sc* dependence ranges from -0.5103 to -0.5454, and that of high *Sc* dependence ranges from -0.8022 to -0.8484. The confidence internal of a *t*-test with 95% confidence interval for the exponent for the low *Sc* dependence is -0.529 ± 0.037, and that of the exponent

Table 1
Correlations of K^+ as a function of Sc for different reaction rates

Reaction probability	$t_{1/2}$ (wall units)	k (wall units)	$Sc \leqslant 10$	$Sc \geqslant 50$
0.1	6.58	0.105	$K^+ = 0.0536\,Sc^{-0.5289}$	$K^+ = 0.1283\,Sc^{-0.8306}$
0.25	2.41	0.288	$K^+ = 0.0540\,Sc^{-0.5454}$	$K^+ = 0.1130\,Sc^{-0.8022}$
0.5	1.00	0.693	$K^+ = 0.0539\,Sc^{-0.5180}$	$K^+ = 0.1164\,Sc^{-0.8030}$
0.75	0.50	1.386	$K^+ = 0.0519\,Sc^{-0.5426}$	$K^+ = 0.1376\,Sc^{-0.8382}$
1.0	0.00	∞	$K^+ = 0.0543\,Sc^{-0.5103}$	$K^+ = 0.1472\,Sc^{-0.8484}$

The reaction probability p is related to the nominal reaction rate constant as follows: $k = \ln(2)/t_{1/2}$, and $t_{1/2} = \ln(0.5)/\ln(1\text{-}p)$

for the high Sc dependence is -0.825 ± 0.026. Eqs. (11a) and (11b) are a key finding of this study. It appears that an important effect of a reactive wall is that the concentration at the wall is not zero, when the reaction rate is not infinite. This fact allows the definition of a mass transfer coefficient based on the difference between the bulk concentration and the wall concentration that, in addition, is not reaction rate dependent.

In the analysis done by Kader and Gukhman [6], it was assumed that $K^+ \sim -2/3$ for $Sc \gg 1$ with the presence of a first-order reaction. The numerical results of Mitrovic et al. [16] predicted $K^+ \sim Sc^{-0.510}$ for $Sc \leqslant 10$ and $\sim Sc^{-0.690}$ for $Sc \geqslant 100$ when there is no reaction and there is a constant mass flux from the wall to the bulk. The experimental measurements of Shaw and Hanratty [32] of the turbulent mass transfer coefficient in channels without reaction and a constant mass flux from the wall to the bulk gave an exponential value of -0.704 for high Sc. The different results of K^+ obtained analytically, experimentally, and numerically address different physical problems. In the study presented here, and the study by Kader and Gukhman [6], the reactants diffuse from the bulk to the wall and react with the wall by a first-order reaction. In the other studies, there was no reaction and the mass markers diffused from the wall to the bulk with a constant mass flux. The net mass flux from the bulk to the wall in the present study is not constant. All of these differences account for the different exponent values of K^+ in different situations.

In order to calculate the mass transfer coefficient for the whole Sc domain, the generalized equation proposed by Churchill and Usagi [33] for all phenomena that have different asymptotic behavior at two limits can be used. According to this generalized equation

$$\frac{K(Sc)}{K_\infty(Sc)} = \left[1 + \left(\frac{K_0(Sc)}{K_\infty(Sc)}\right)^n\right]^{1/n} \tag{12}$$

where K_∞ (Sc) and $K_0(Sc)$ represent asymptotic expressions for large and small values of Sc, respectively, which are given by Eqs. (11a) and (11b) For more details of how to implement this generalized method, refer to Churchill and Usagi [33] and Mitrovic et al. [16]. In order to satisfy this condition with 99% accuracy, n has to be negative with high absolute value $(n \leqslant -11)$. By choosing $n = -13.528$, the following expression was derived using Eq. (12), which gives excellent approximation for data with $Sc \leqslant 10$ or $Sc \geqslant 100$, (and presumably good approximations for data with $10 \leqslant Sc \leqslant 100$):

$$K^+ = \frac{0.1285\,Sc^{-0.8245}}{\left[1 + \left(\frac{19.348}{Sc}\right)^4\right]^{0.074}} \tag{13}$$

This correlation was plotted together with the data points and is shown in Fig. 6.

4.3. Effective reaction rate constant

The effective reaction rate constant, k_{eff}, is the rate constant of the reaction taking place on the channel wall. The effective reaction rate constant, k_{eff}, can be calculated using Eq. (3). Fig. 7 shows the ratio of the effective reaction rate constant with any p divided by the effective reaction rate constant for an instantaneous reaction, $k_{\text{eff}}/k_{\text{eff}(p\,=\,1.0)}$, along the length of the channel for the cases of a low Sc $(Sc = 0.7)$ and a high Sc $(Sc = 100)$. It can be seen that k_{eff} increases with higher p, as expected. Also, the ratio $k_{\text{eff}}/k_{\text{eff}\,(p=1.0)}$ in the low Sc case is smaller than in the high Sc case. This indicates that the reaction probability has a stronger effect in lower Sc flows. For higher Sc flows, the rate of diffusion of reactants to the wall is very slow and the reaction is diffusion limited. Therefore, when p increases, k_{eff} does not increase with the same rate in higher Sc flows. In Fig. 7b, all the curves turn higher and approach 1 as x^+ increases. This indicates that the reactions become more and more diffusion limited downstream.

4.4. Flow effects on reaction

A probability, p_P, can be defined that any mass marker at a specific time step in the flow field will react with the

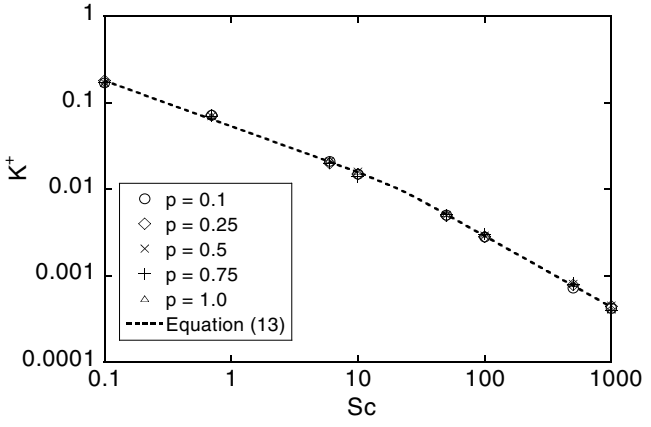

Fig. 6. Generalized correlation for the mass transfer coefficient as a function of the Schmidt number and comparison to data.

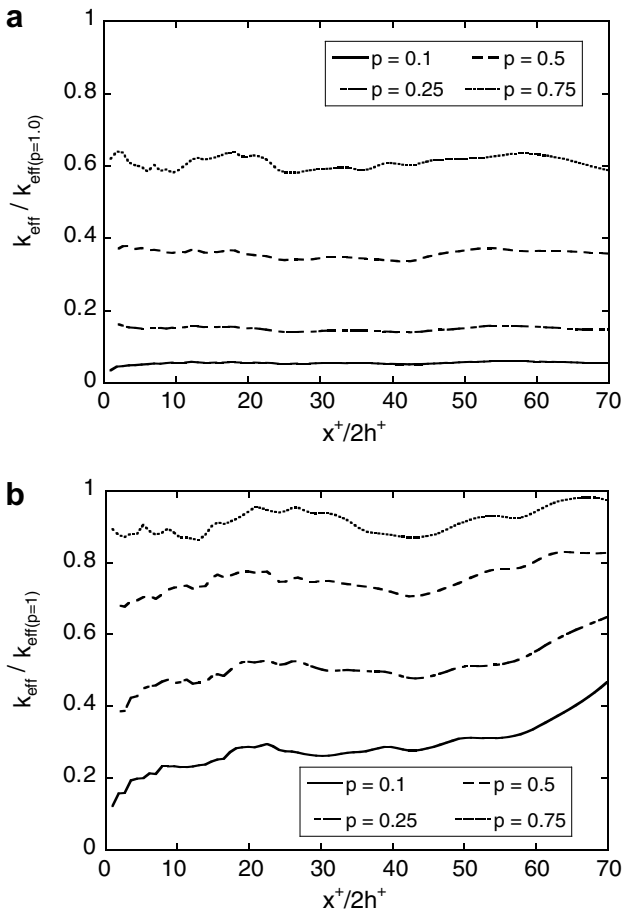

Fig. 7. Effective reaction rate constant as a fraction of the effective rate constant for the case of an instantaneous reaction ($p = 1.0$) for (a) $Sc = 0.7$, and (b) $Sc = 100$.

wall. This probability density function is different from the reaction probability, p, which is a binomial probability density function that a mass marker colliding with the wall reacts. In other words, p is proportional to the nominal reaction rate, and p_P is proportional to the effective reaction rate. At time step t,

$$p_P = (\text{number of reactions at time step } t) / (\text{number of mass markers at time step } t) \quad (14a)$$

$$p = (\text{number of reactions at time step } t) / (\text{number of collisions with the wall at time step } t) \quad (14b)$$

Fig. 8 shows the ratio p_P/p as a function of p and Sc. This ratio is actually the probability that any mass marker in the flow field at a specific time step collides with the wall

$$p_P/p = (\text{number of collisions at timestep } t) / (\text{number of mass markers at time step } t) \quad (15)$$

This ratio demonstrates the effect of the flow on the reaction. Without flow, for a first-order reaction, all the markers would have a chance to react in every time step, and the ratio would have been equal to one. As shown in

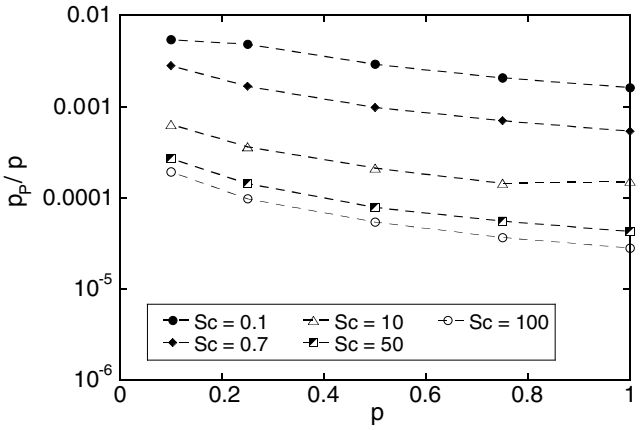

Fig. 8. Ratio of effective reaction rate over nominal reaction rate for different Sc.

the figure, p_P/p increases with lower Sc and lower p. The mass markers have larger random motions in lower Sc flows, and, therefore, can diffuse to the wall faster, increasing the collision probability. When p is higher, the reaction happens faster and the bulk concentration decreases quickly. This will result in a lower concentration gradient between the bulk and the wall, and, therefore, it will lower the diffusion rate of the mass markers to the wall, which results in lower collision probability.

4.5. Individual marker statistics

Statistical values characterizing individual marker trajectories, like the mean surviving distance and the surviving probability as a function of time, are plotted in Figs. 9 and 10 for the case of instantaneous reaction ($p = 1.0$). The surviving distance is defined as the total distance that a marker travels before it gets adsorbed by the wall [34]. The mean surviving distance is the average of all the surviving distances traveled by all the markers that have reacted. The surviving probability is the ratio of the number of non-

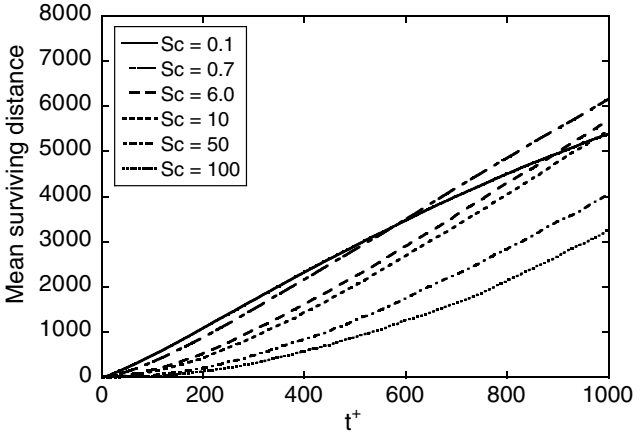

Fig. 9. The mean surviving distance as a function of time. The mean surviving distance at a specific time is the average total distance traveled (in all directions) by the markers that have reacted by that time.

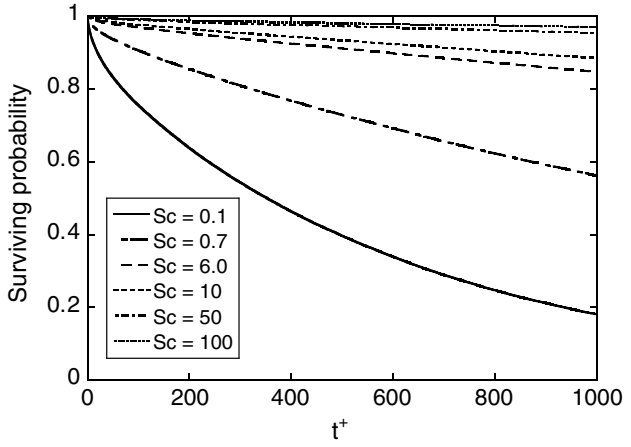

Fig. 10. The surviving probability as a function of time. The surviving probability at a time is the percentage of non-reacted markers divided by the total number of markers released up to that specific time.

reacted markers over the total number of makers released [34], and it is an indication of the conversion of the reactants (conversion is equal to the percentage of molecules reacted divided by the total molecules that entered the flow, i.e., equal to 100% minus the surviving probability). The surviving probability is related to the reactor length required to achieve a specific conversion. For example, the time step at which the surviving probability is 50% can be multiplied by the bulk velocity of the flow to obtain the reactor length necessary for 50% conversion.

It can be seen that Sc has a strong effect on the mean surviving distance. In low Sc flows, the markers have larger random molecular motions and, therefore, the distances traveled by the markers are farther than those in high Sc flows. However, in low Sc flows, the markers have a higher chance to collide and react with the wall. As a result, for low Sc flows, the mean surviving distance curve will go up faster initially and approach a plateau later in time, when most of the markers have reacted, as shown in Fig. 9. Fig. 10 indicates how fast the reaction occurs for different Sc flows. At $t^+ = 1500$, more than 90% of the markers have reacted for $Sc = 0.1$, while only 5% of the markers have reacted for $Sc = 1000$.

5. Conclusions

The interactions of a first-order reaction and turbulent mass transfer were investigated. Because of the accumulation of slow moving reactants near the wall and the way the reactants are released into the flow field, the mass concentration is much higher near the walls than in the bulk in the entrance-effect region. The length of the entrance-effect region increases with higher Sc and lower reaction rate. Beyond the entrance-effect region, the effects of the surface reaction dominate and the flow is stabilized.

In the stabilized region, it was found that the reaction is diffusion limited for large Sc (50 and above). The mass transfer coefficient was found to be independent of the reaction rate, but to be strongly dependent on Sc given by Eqs. (11a) and (11b) for the asymptotic cases for low and high Sc, respectively. A generalized correlation that can predict the mass transfer coefficient for the whole range of Sc is given in Eq. (13). The mass transfer to the wall is not enhanced by a faster surface reaction, contrary to the case of mass transfer from the wall followed by a first-order reaction. In the case presented here, the mass transfer depends on the diffusion of the reactant to the wall due to turbulence and due to molecular means. The effective reaction rate increases with higher nominal rate of reaction. The nominal reaction rate, which is proportional to the probability of having a reaction when a marker collides with the wall, has a stronger effect for lower Sc fluids. The effects of the flow on the reaction are to decrease the reaction rate. High Sc fluids and faster reactions are affected the most. Finally, the survival probability of reactant markers within the flow field has been calculated, which can be directly related to the length of a reactor needed to achieve a specific conversion.

Acknowledgements

The support of NSF under CTS-0209758 and CBET-0651180 is gratefully acknowledged. This work was also supported by the National Computational Science Alliance under CTS-040023 and utilized the NCSA IBMp690.

References

[1] J. Xaman, G. Alvarez, Effect of heat conduction on SnS–Cu_xS solar control coated semitransparent wall on turbulent natural convection in a square cavity, Numer. Heat Transfer A 50 (1) (2006) 79–98.
[2] N. Yucel, N. Dinler, Numerical study of laminar and turbulent flow through a pipe with fins attached, Numer. Heat Transfer A 49 (1) (2006) 195–214.
[3] J.-H Kim, K.E. Jansen, M.K. Jensen, Simulation of three-dimensional incompressible turbulent flow inside tubes with helical fins, Numer. Heat Transfer B 46 (3) (2004) 95–221.
[4] T.S. Park, Numerical study of turbulent flow and heat transfer in a convex channel of a calorimetric rocket chamber, Numer. Heat Transfer A 45 (10) (2004) 1029–1047.
[5] Y. Na, Direct numerical simulation of turbulent scalar field in a channel with wall injection, Numer. Heat Transfer A 47 (2) (2005) 165–181.
[6] B.A. Kader, A.A. Gukhman, Turbulent mass transfer with a first-order chemical reaction on a wall at $Pr \gg 1$, Int. J. Heat Mass Transfer 20 (1977) 1339–1350.
[7] O.T. Hanna, O.S. Sandall, C.L. Wilson, Mass transfer accompanied by first-order chemical reaction for turbulent duct flow, Ind. Eng. Chem. Res. 26 (1987) 2286–2290.
[8] E.S.C. Meyerink, S.K. Friedlander, Diffusion and diffusion controlled reactions in fully developed turbulent pipe flow, Chem. Eng. Sci. 17 (1962) 121–135.
[9] R. Harriott, R.M. Hamilton, Solid–liquid mass transfer in turbulent pipe flow, Chem. Eng. Sci. 20 (1965) 1073–1078.
[10] J.J. Riley, R.W. Metcalfe, S.A. Orszag, Direct numerical simulation of chemically reacting mixing layer, Phys. Fluids 29 (2) (1986) 407–422.
[11] A.D. Leonard, J.C. Hill, Direct numerical simulation of turbulent flows with chemical reaction, J. Sci. Comput. 3 (1998) 25–43.

[12] B.M. Mitrovic, D.V. Papavassiliou, Effects of a first-order chemical reaction on turbulent mass transfer, Int. J. Heat Mass Transfer 47 (1) (2004) 43–61.
[13] A.E. Amiri, S.K. Hannani, F. Mashayek, Large-eddy simulation of heavy-particle transport in turbulent channel flow, Numer. Heat Transfer B 50 (4) (2006) 285–313.
[14] S.W. Churchill, Interaction of chemical reactions and transport. 1. An overview, Ind. Eng. Chem. Res. 44 (2005) 5199–5212.
[15] S.W. Churchill, B. Yu, Effects of transport on reactions in homogeneous tubular flow, Ind. Eng. Chem. Res. 45 (25) (2006) 8583–8593.
[16] B.M. Mitrovic, P.M. Le, D.V. Papavassiliou, On the Prandtl or Schmidt number dependence of the turbulence heat or mass transfer, Chem. Eng. Sci. 59 (2004) 543–555.
[17] K. Kontomaris, T.J. Hanratty, J.B. McLaughlin, An algorithm for tracking fluid particles in a spectral simulation of turbulent channel flow, J. Comp. Phys. 103 (1993) 231–242.
[18] A. Einstein, Uber die von der molecular-kinetischen theorie der Warme geforderte Bewegung von in ruhenden Flussigkeiten suspendierten Teilchen, Ann. Phys. 17 (1905) 549.
[19] D.V. Papavassiliou, T.J. Hanratty, The use of Lagrangian methods to describe turbulent transport of heat from the wall, Ind. Eng. Chem. Res. 34 (1995) 3359–3367.
[20] D.V. Papavassiliou, T.J. Hanratty, Transport of a passive scalar in a turbulent channel flow, Int. J. Heat Mass Transfer 40 (6) (1997) 1303–1311.
[21] S.S. Ponoth, J.B. McLaughlin, Numerical simulation of mass transfer for bubbles in water, Chem. Eng. Sci. 55 (2000) 1237–1255.
[22] D.V. Papavassiliou, Scalar dispersion from an instantaneous line source at the wall of a turbulent channel for medium and high Prandtl number fluids, Int. J. Heat Fluid Flow 23 (2002) 161–172.
[23] D.V. Papavassiliou, Turbulent transport from continuous sources at the wall of a channel, Int. J. Heat Mass Transfer 45 (17) (2002) 3571–3583.
[24] Y. Mito, J.J. Hanratty, Lagrangian stochastic simulation of turbulent dispersion of heat markers in a channel flow, Int. J. Heat Mass Transfer 46 (6) (2003) 1063–1073.
[25] B.M. Mitrovic, D.V. Papavassiliou, Transport properties for turbulent dispersion from wall sources, AICHE J. 49 (5) (2003) 1095–1108.
[26] P.M. Le, D.V. Papavassiliou, Turbulent dispersion from elevated line sources in plane channel and plane Couette flow, AICHE J. 51 (9) (2005) 2402–2414.
[27] P.M. Le, D.V. Papavassiliou, On temperature prediction at low Re turbulent flows using the Churchill turbulent heat flux correlation, Int. J. Heat Mass Transfer 49 (2006) 3681–3690.
[28] P.M. Le, D.V. Papavassiliou, Turbulent heat transfer in plane Couette flow, J. Heat Transfer Trans. ASME 128 (2006) 53–62.
[29] J.E. Cermak, Lagrangian similarity hypothesis applied to diffusion in turbulent shear flow, J. Fluid Mech. 15 (1963) 29–64.
[30] S.L. Lyons, T.J. Hanratty, J.B. McLaughlin, Large-scale computer-simulation of fully-developed turbulent channel flow with heat-transfer, Int. J. Numer. Methods Fluids 13 (8) (1991) 999–1028.
[31] A. Gunther, D.V. Papavassiliou, M.D. Warholic, T.J. Hanratty, Turbulent flow in channel at low Reynolds number, Exp. Fluids 25 (1998) 503–511.
[32] D.A. Shaw, T.J. Hanratty, Turbulent mass transfer rates to a wall for large Schmidt numbers, AICHE J. 23 (1) (1977) 28–37.
[33] S.W. Churchill, R. Usagi, A general expression for the correlation of rates of transfer and other phenomena, AIChE J. 18 (1972) 1121–1127.
[34] M.M. Tomadakis, D. Rupani, Diffusion controlled reaction rate, survival probability, and molecular trajectory characteristics in the bulk, transition and Knudsen regime, Chem. Eng. J. 128 (1) (2007) 1–10.